Optimizing PRESS Localized Citrate Detection at 3 Tesla

Andreas H. Trabesinger,[1] Dieter Meier,[1] Ulrike Dydak,[1] Rolf Lamerichs,[2] and Peter Boesiger[1]*

Analytical methods are used to characterize the response of the strongly coupled two-spin system of citrate to point-resolved spectroscopy (PRESS)-based sequences at 3 T. The signal output is analyzed line by line, as well as in the Cartesian product operator basis. Patterns with a periodicity of 80.9 ms are identified. Furthermore, it is shown that at TE = $n \cdot 80.9$ *ms* ($n \in \{0,1,2,\ldots\}$), the spin evolution can be described without direct reference to strong coupling terms. The theoretical results are found to be in good agreement with in vivo experiments. These results can be used to design protocols for prostate MRS and MRSI at 3 T, and give guidelines for optimizing spin-echo-based acquisition schemes for detecting two-spin systems at arbitrary field strengths. Magn Reson Med 54:51–58, 2005. © 2005 Wiley-Liss, Inc.

Key words: strong coupling; citrate; PRESS; 3 Tesla; prostate; MRS

Monitoring the levels of metabolites serves as an indispensable source of biochemical information about the normo- and pathophysiological state of human organs. Whereas most methods for assessing metabolic levels are invasive in nature, magnetic resonance spectroscopy (MRS) and magnetic resonance spectroscopic imaging (MRSI) allow information to be acquired in a fully noninvasive way (1). These modalities are predominantly used for the study of the brain; however, since the early 1990s in vivo MRS has been shown to be extremely useful for opening a window into the metabolism of the human prostate (for a recent review see Ref. 2 and references therein).

From a biochemical point of view, the capability provided by ^{1}H MRS to monitor citrate levels is of particular interest. The role of citrate in prostate metabolism is well understood (2). In brief, healthy prostate epithelial cells are known to synthesize and secrete citrate in relatively large amounts (~60 mmol/l). The high levels of zinc in the healthy prostate inhibit the oxidation of citrate in the Krebs cycle. However, in cancerous epithelial cells, zinc levels are drastically reduced, resulting in decreased production and secretion of net citrate in tumor cells. Therefore, monitoring citrate levels in the prostate provides direct biochemical information for the differential diagnosis of malignant adenocarcinoma vs. benign prostate hyperplasia. In MRI studies, unambiguous differentiation is difficult to obtain; however, the combination of MRI and MRS/MRSI is a very promising approach for achieving that goal (2).

The observed ^{1}H MRS signal of citrate ($^-$OOC-CH_2-C(O-H)(COO^-)-CH_2-COO^-) arises from its two magnetically equivalent CH_2 moieties that resonate around 2.6 ppm. The two protons of each methylene group are magnetically inequivalent. Under physiological conditions their Larmor frequencies differ by 0.147 ppm, while the *J*-coupling strength between them is $J = 16.1$ Hz (3). At currently available fields for in vivo MRS studies ($\leq$7 T), the difference in Larmor frequencies is comparable to *J*. Therefore citrate constitutes a strongly coupled AB spin system, and consequently its response to a given pulse sequence is field-dependent.

During the past decade, several groups thoroughly optimized the acquisition schemes that are commonly used in localized in vivo spectroscopy for citrate acquisition (4–12). The problem at hand is to tune the acquisition scheme to yield an intense signal whose lineshape allows reliable quantification. Since spectral overlap with other resonance lines does not present a major problem, spectral selectivity is not a prime demand.

The double spin-echo method called point-resolved spectroscopy (PRESS) (13) has become the main tool of researchers in prostate MRS. This is mainly due to the high inherent signal yield of PRESS compared to, e.g., the stimulated-echo acquisition mode (STEAM) method (14). Moreover, it is more amendable in terms of sequence optimization. While the optimal timing of the PRESS sequence was explored experimentally in pioneer studies (4), it was soon realized that a more general approach would be to use analytical calculations to predict the signal output (5). Aided by the increasing power of computer algebra, analytical methods have been extensively used to optimize PRESS localized citrate detection at 1.5 T, and this field strength has constituted the "gold standard" for clinical applications for far more than a decade.

In the past few years, compact MR systems that operate at 3 T have become available for both research and clinical use. The higher field provides increased polarization, improved detection sensitivity, and higher chemical shift dispersion. The pelvic region is only marginally affected by respiratory and cardiac motion, which facilitates prostate MRS. However, it is difficult to access the prostate from the surface of the body. The use of endorectal coils has brought considerable improvement (15–17), albeit at the cost of patient discomfort and potential problems associated with signal hyperintensities close to the coil, as well as with mechanical pressure on the periphery of the prostate. Surface coils (and arrays thereof) avoid these problems, but suffer on their part from lower sensitivity.

[1]Institute for Biomedical Engineering, ETH Zurich and University of Zurich, Zurich, Switzerland.

[2]Philips Medical Systems, Best, The Netherlands.

Grant sponsor: ETH Zurich (Strategic Excellence Project); Grant number: SEP TH 7/02-2.

Andreas H. Trabesinger's current address is the Laboratory of Physical Chemistry, ETH Zurich, Zurich, Switzerland.

*Correspondence to: Prof. Dr. P. Boesiger, Institute of Biomedical Engineering, University and ETH Zurich, Gloriastrasse 35, CH-8092 Zurich, Switzerland. E-mail: boesiger@biomed.ee.ethz.ch

Received 22 July 2004; revised 9 February 2005; accepted 10 February 2005.

DOI 10.1002/mrm.20544

Published online in Wiley InterScience (www.interscience.wiley.com).

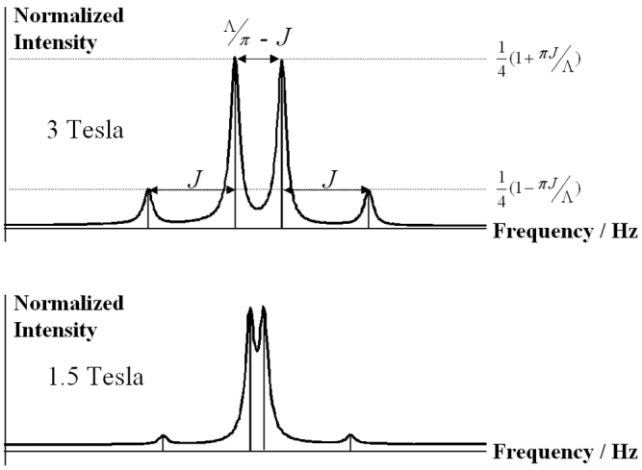

FIG. 1. Sketch of the citrate signal as obtained in a pulse-acquire experiment at 1.5 T (bottom) and 3 T (top). J denotes the strength of the J-coupling in Hz; $\Lambda = \sqrt{(\pi\Delta\nu)^2 + (\pi J)^2}$, where $\Delta\nu$ is the difference in Larmor frequencies between the two unequivalent protons in Hz. The total intensity is one.

The increased signal available at high field strengths, however, makes surface-detected prostate MRS more attractive.

In this communication we present a systematic study aimed at optimizing the timing of PRESS-based acquisition schemes for the detection of citrate at 3 T. Full analytical expressions are given. These can be used to describe the response of any two-spin system to the PRESS sequence at arbitrary fields.

THEORY

The spectrum of the AB spin system consists of four lines. Their positions and relative intensities are indicated in Fig. 1 for citrate at 1.5 T and 3 T. The displayed spectra correspond to the signal detected in a pulse-acquire experiment. Inserting the J-coupling values and chemical shift differences as determined by van der Graaf and Heerschap (3) (J = 16.1 Hz, chemical shift difference $\Delta\nu$ = 0.147 ppm), the separation of the inner two lines is found to be 2.5 Hz at 1.5 T and 8.6 Hz at 3 T, while the separation of the leftmost two lines and the rightmost two lines is 16.1 Hz independently of field strength. The relative intensities of the inner and outer lines scale with field: whereas at 1.5 T 93.2% of the total signal energy is concentrated in the inner lines, this percentage decreases to 82.5% at 3 T.

For the purpose of this study, we model the PRESS sequence as a series of two spin echoes ($[90°]_x - t_1/2 - [180°]_y - t_1/2 - t_2/2 - [180°]_y - t_2/2 - \mathrm{Acq}$) induced by delta pulses of infinite bandwidth. In this simplified picture, t_1 and t_2 are the only adjustable parameters. Under these assumptions, analytical expressions can be given for the response of the citrate spins to the PRESS sequence. This model is expected to produce useful starting values for an optimization process. When non-ideal pulses with accompanying slice-selection gradients are to be included, one typically has to resort to numerical methods (18).

The effect of the PRESS sequence can be described as changing the intensities and phases of the four lines, but of course not their frequency positions. The mirror symmetry of the whole spectrum about the centerline will be preserved throughout the evolution, and therefore only one of the inner and one of the outer lines are considered in the following. The shape of one individual line can be completely described as a linear combination of an absorption and a dispersion lineshape. Knowing the intensities as well as the relative contributions of absorption and dispersion components to the inner and outer lines, respectively, allows one to fully predict the spectrum resulting from a specific choice of t_1 and t_2.

This approach corresponds to expressing the density matrix that describes the AB spin system in a basis set sorted by the transition frequencies. Working on this line-by-line basis yields all characteristics of the citrate spectrum obtained in response to an ideal PRESS sequence. However, it does not provide comprehensive insight into the evolution of the spin system. Product operators (19) represent a basis set that gives a more intuitive understanding of the underlying physical mechanisms. While the original description (19) assumed weak coupling, Kay and McClung (20) extended the theory to strongly coupled AB and ABX spin systems. In spin-echo sequences based on 180° rotations for signal refocusing, only the magnetization components (i.e., single quantum coherences) are of interest. Therefore, only eight of the 16 basis vectors for a two-spin system need to be considered. Symmetry arguments allow these vectors to be grouped in four sets: in-phase magnetization ($A_y + B_y$) and ($A_x - B_x$), and anti-phase magnetization ($2A_xB_z + 2A_zB_x$) and ($2A_yB_z - 2A_zB_y$). As in the single transition basis, the signal output is again characterized by four basis vectors. For comparison, a weakly coupled system exclusively evolves into terms of the form ($A_y + B_y$) and ($2A_xB_z + 2A_zB_x$) (19). The occurrence of terms of the form ($A_x - B_x$) and ($2A_yB_z - 2A_zB_y$) in the density matrix is specific to strongly coupled systems, and is due to the fact that there is an oscillatory transfer of magnetization between the A and B spins. This transfer is quenched in the weak coupling limit. These facts motivate our choice of the two subspaces {($A_y + B_y$), ($2A_xB_z + 2A_zB_x$)} and {($A_x - B_x$), ($2A_yB_z - 2A_zB_y$)} for expressing the results below.

In the following text we use both basis sets (single transition operators and product operators) to identify suitable parameter sets for citrate detection at 3 T. The goals of our design strategy were to 1) channel the signal into one pair of lines, and 2) obtain pure absorptive signals with no contamination from dispersive contributions. These criteria facilitate the identification and quantification of the citrate peaks, and minimize the risk of mutual signal cancellation in cases in which the linewidth becomes comparable to the separation of the individual lines of the multiplet.

MATERIALS AND METHODS

All of the algebraic calculations were performed using a Mathematica (Wolfram Research, Champaign, IL, USA) implementation of the product operator formalism for strongly coupled AB spin systems (20). To calculate the

Table 1
Absorption and Dispersion Contributions to the Inner and Outer Lines in Response to the PRESS Sequence ($[90°]_x - t_1/2 - [180°]_y - t_1/2 - t_2/2 - [180°]_y - t_2/2 - Acq$)*

	Absorption	Dispersion
Inner	$(\pi J)^2(\Lambda + \pi J)\cos[(\Lambda - \pi J)TE] + \delta^2(\Lambda + \pi J)\cos[\pi J \cdot TE] + 2\delta^2\pi J \sin\left[\frac{1}{2}\Lambda \cdot TE\right]\sin\left[\pi J \cdot TE + \frac{1}{2}\Lambda(t_1 - t_2)\right]$	$-(\pi J)^2(\Lambda + \pi J)\sin[(\Lambda - \pi J)TE] + \delta^2(\Lambda + \pi J)\sin[\pi J \cdot TE] - 2\delta^2\pi J \sin\left[\frac{1}{2}\Lambda \cdot TE\right]\cos\left[\pi J \cdot TE + \frac{1}{2}\Lambda(t_1 - t_2)\right]$
Outer	$(\pi J)^2(\Lambda - \pi J)\cos[(\Lambda + \pi J)TE] + \delta^2(\Lambda - \pi J)\cos[\pi J \cdot TE] + 2\delta^2\pi J \sin\left[\frac{1}{2}\Lambda \cdot TE\right]\sin\left[\pi J \cdot TE - \frac{1}{2}\Lambda(t_1 - t_2)\right]$	$-(\pi J)^2(\Lambda - \pi J)\sin[(\Lambda + \pi J)TE] - \delta^2(\Lambda - \pi J)\sin[\pi J \cdot TE] + 2\delta^2\pi J \sin\left[\frac{1}{2}\Lambda \cdot TE\right]\cos\left[\pi J \cdot TE - \frac{1}{2}\Lambda(t_1 - t_2)\right]$

*J denotes the strength of the J-coupling in Hz: $\delta = \frac{1}{2}\Delta\omega$, where $\Delta\omega = 2\pi\,\Delta\nu$ and $\Delta\nu$ is the difference in Larmor frequencies in Hz: $\Lambda = \sqrt{\delta^2 + (\pi J)^2}$; $TE = t_1 + t_2$.

single line characteristics, a single transition basis was chosen within the same framework.

In vivo experiments were performed on a Philips Intera 3.0 T system (Philips Medical Systems, Best, The Netherlands). The study complied with the regulations of the local ethics committee. The spectra of three healthy volunteers (24–53 years old) were acquired from volumes varying between 9.0 and 12.4 ml that were defined in the central part of the prostate. A single-element surface coil (rectangular, 10 cm × 20 cm) was used in combination with body coil transmission. Sixty-four to 512 scans were averaged at TR = 1.2 s. Water signal was suppressed using band-selective inversion with gradient dephasing (BASING) refocusing (21), and fat suppression was accomplished by a frequency-selective inversion recovery prepulse, which was found to have no effect on the citrate signal. The inversion time was optimized in each experiment. The manufacturer's default PRESS implementation was used, in which the first TE (t_1) is made as short as possible to render the PRESS sequence as asymmetric as possible to avoid stimulated echoes. In our experiments the minimum t_1 was 28 ms, and was limited essentially by the length of the RF pluses. Postprocessing was restricted to DC correction and exponential apodization corresponding to 1.5 Hz line-broadening.

RESULTS

We present the results of our analysis in two parts: First, the spectrum obtained in response to the PRESS sequence is characterized line by line. Second, the same signal is described in the product operator basis. In each part, we first present the full analytical expressions in a compact form, and then discuss typical features by considering specific examples.

The amplitudes for the absorptive and dispersive contributions to the inner and outer lines in dependence on t_1 and t_2 are given in Table 1. Each of the four amplitudes is described by a sum of three terms. Only the last one of these three terms depends on the degree of asymmetry of the PRESS sequence, i.e., on $(t_1 - t_2)$. The other two terms depend exclusively on the total TE $(t_1 + t_2)$. Each of the three terms contributes significantly to the citrate spectrum at 3 T.

As a typical example, we plot in Fig. 2 the individual contributions as a function of t_2 for a PRESS sequence with the first TE (t_1) fixed at 28.0 ms. This corresponds to the PRESS implementation that was used for the in vivo experiments presented below, where as usual the first TE was made as short as possible. As previously pointed out by Schick et al. (4), the outer lines are subject to faster oscillations than the inner lines. Furthermore, it is apparent that the total signal energy oscillates between the inner

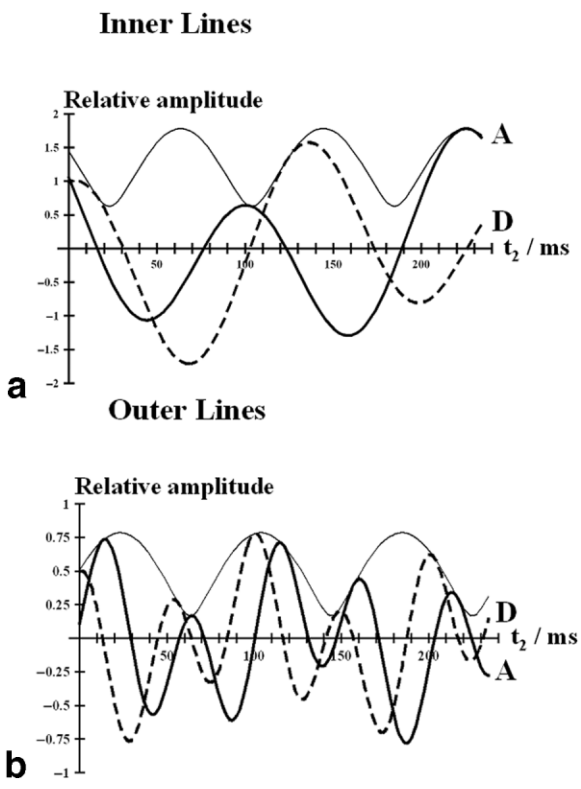

FIG. 2. Contributions to the citrate signal in response to the PRESS sequence ($[90°]_x - t_1/2 - [180°]_y - t_1/2 - t_2/2 - [180°]_y - t_2/2 - Acq$). The signals are displayed as a function of t_2, while t_1 is fixed at 28.0 ms. **a:** Signal of the inner lines. **b:** Signal of the outer lines. Bold solid line: absorption component (A); dashed line: dispersion component (D); thin solid line: total intensity $\sqrt{A^2 + D^2}$.

and outer lines. The period of this transfer is $2\pi/\Lambda$, where $\Lambda = [(\pi\Delta\nu)^2 + (\pi J)^2]^{1/2}$. At 3 T, this characteristic time is 80.9 ms. In the present example, the first maximum of the inner lines intensity occurs at t_2 = 23.0 ms + π/Λ = 63.4 ms. At this time the outer line's intensity has its first minimum. The position of these extrema (but not the period length) along t_2 depends on the choice of t_1. This point will be revisited later.

The design strategy defined above involves channeling the signal energy into a single pair of lines. Since the inner two lines reach stronger maximum intensities, we focus on this pair. The maxima of the total intensity are found in our example at t_2 = 63.4 ms + n · $2\pi/\Lambda$ ($n \in \{1,2,3,\ldots\}$), i.e., at t_2 = 63.4 ms, t_2 = 144.3 ms, t_2 = 225.2 ms, etc.). At the first two maximum positions (corresponding to TE = 91.4 ms and TE = 172.3 ms) the shape of the inner lines has strong dispersion components (cf., Fig. 2a). At the time of the third maximum (TE = 253.2 ms), however, the lineshape is almost completely absorptive, as desired.

As stated above, the position of the extrema in total intensity along t_2 depends on the value of t_1. The optimal choice is $t_1 = 2\pi/\Lambda$ = 80.9 ms. With this setting the maxima in the total intensity of the inner lines occur at the earliest time. The first maximum is then at t_2 = 0 ms (which of course is not practical) and further maxima follow at $n \cdot 2\pi/\Lambda$ ($n \in \{1,2,3,\ldots\}$), i.e., at t_2 = 80.9 ms, t_2 = 161.7 ms, etc., corresponding to TE values of TE = 161.7 ms, TE = 242.6 ms, etc.). This means that the favorable spectral appearance described above can already be found at TE = $t_1 + t_2$ = 80.9 ms + 161.7 ms = 242.6 ms.

To demonstrate the "good" properties of this sequence timing, we show in Fig. 3 the parametric plots of the trajectory of the inner lines, and the outer lines' signal through the space of possible lineshapes as TE is increased from 0 to 6 · $2\pi/\Lambda$ (see figure caption). This is of course nothing else than the trajectories of the inner lines', and the outer lines' magnetization in the transverse plane. Consider again the inner lines: We start with purely absorptive, positive lines (at t = 0). The trajectory then passes through smaller values of total intensity (i.e., smaller radii), and touches the line of maximum intensity at $t = t_1 = 2\pi/\Lambda$ (i.e., at t_2 = 0). At these times, strong dispersive components contribute to the signal. The same is true for the second maximum at $t = 4\pi/\Lambda$ (i.e., at $t_2 = 2\pi/\Lambda$). At $t = 6\pi/\Lambda$ (i.e., at $t_2 = 4\ \pi/\Lambda$), we are almost back to the starting point, where strong nearly purely absorptive inner lines are obtained.

Additional insight can be gained if the same results are expressed on a Cartesian product operator basis. The corresponding analytical expressions are given in Table 2. Figure 4 shows parametric plots of the trajectories, but now in the spaces defined above: $\{X^+,Y^+\} \equiv \{(A_y + B_y), (2A_xB_z + 2A_zB_x)\}$ and $\{X^-,Y^-\} \equiv \{(A_x - B_x), (2A_yB_z - 2A_zB_y)\}$. We find that at total echo times (TEs) = n · $^{2\pi}/_{\Lambda}$ ($n \in \{1,2,3,\ldots\}$) only terms in $\{X^+,Y^+\}$ are nonzero. This finding holds independently of the specific choice for t_1, i.e., the position of these points depends solely on the total TE. In contrast, the trajectory between these points changes according to the setting of t_1 for a fixed value of TE.

As mentioned above, $\{X^+,Y^+\}$ represents the space where a weakly coupled two-spin system would "live" during evolution under the PRESS sequence. Therefore, at

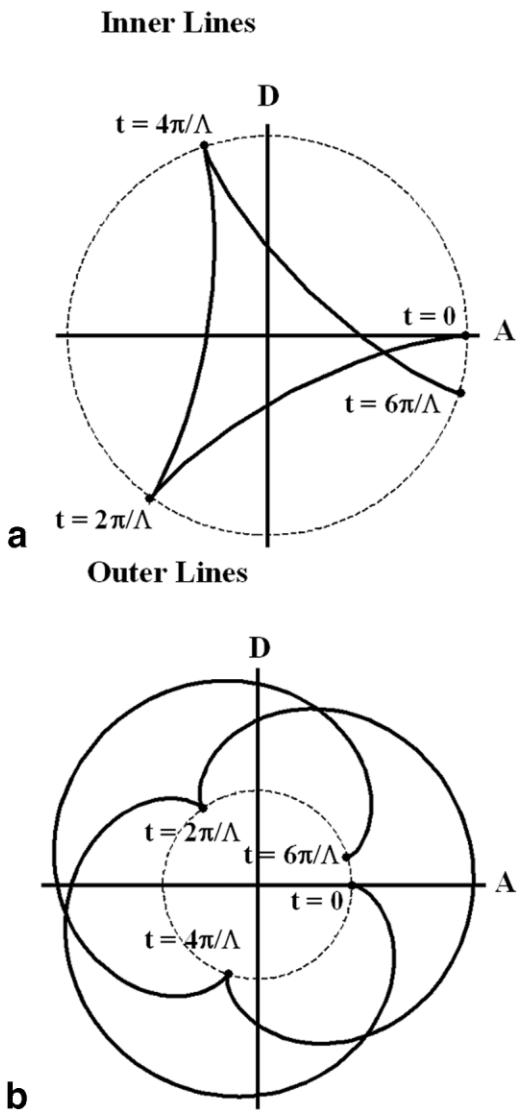

FIG. 3. Parametric plots of the trajectory through the space of possible lineshapes for the signal of the inner lines (**a**) and the signal of the outer lines (**b**). For $0 \le t \le 2\pi/\Lambda$, t_1 = t and t_2 = 0; for $2\pi/\Lambda \le t \le 6\pi/\Lambda$, $t_1 = 2\pi/\Lambda$ and $t_2 = t - 2\pi/\Lambda$. Therefore, $t = 6\pi/\Lambda$ corresponds to a PRESS sequence with $t_1 = 2\pi/\Lambda$ = 80.9 ms and $t_2 = 4\pi/\Lambda$ = 161.8 ms. The dashed circles are the lines of equal intensity as at t = 0.

the specific TEs $n \cdot 2\pi/\Lambda$ ($n \in \{1,2,3,\ldots\}$) the spin system behaves as if it was weakly coupled. For these values of TE, the density matrix ρ is (cf. Table 2)

$$\rho(TE = n \cdot 2\pi/\Lambda) = -(A_y + B_y) \cdot \cos[2\pi \cdot n \cdot \pi J/\Lambda] + (2A_xB_z + 2A_zB_x) \cdot \sin[2\pi \cdot n \cdot \pi J/\Lambda]. \quad [1]$$

For comparison, for a weakly coupled two-spin system we obtain

$$\rho(TE) = -(A_y + B_y) \cdot \cos[\pi J \cdot TE] + (2A_xB_z + 2A_zB_x) \cdot \sin[\pi J \cdot TE] \quad [2]$$

for all values of TE.

Table 2
Contributions of the Four Groups of Cartesian Single-Quantum Coherence Product Operators to the PRESS Signal*

Operator	Amplitude
$(A_y + B_y)/2$	$-\cos(\pi J\cdot TE)\cdot\left[\left(\frac{\delta}{\Lambda}\right)^2+(\pi J/\Lambda)^2\cos(\Lambda\cdot TE)\right]$ $-\sin(\pi J\cdot TE)\cdot\left[\left(\frac{\pi J}{\Lambda}\right)^3\sin(\Lambda\cdot TE)+(2\pi J\delta^2/\Lambda^3)\sin\left(\frac{1}{2}\Lambda\cdot TE\right)\cos\left(\frac{1}{2}\Lambda\cdot(t_1-t_2)\right)\right]$
$(2A_xB_z + 2A_zB_x)/2$	$-\cos(\pi J\cdot TE)\cdot\left[\left(\frac{\pi J}{\Lambda}\right)^3\sin(\Lambda\cdot TE)+(2\pi J\delta^2/\Lambda^3)\sin\left(\frac{1}{2}\Lambda\cdot TE\right)\cos\left(\frac{1}{2}\Lambda\cdot(t_1-t_2)\right)\right]$ $+\sin(\pi J\cdot TE)\cdot\left[\left(\frac{\delta}{\Lambda}\right)^2+\left(\frac{\pi J}{\Lambda}\right)^2\cos(\Lambda\cdot TE)\right]$
$(A_x - B_x)/2$	$-\cos(\pi J\cdot TE)\cdot\left[(\pi^2J^2\delta/\Lambda^3)\left(2\sin\left(\frac{1}{2}\Lambda\cdot TE\right)\cos\left(\frac{1}{2}\Lambda\cdot(t_1-t_2)\right)-\sin(\Lambda\cdot TE)\right)\right]$ $-\sin(\pi J\cdot TE)\cdot\left[(2\pi J\delta/\Lambda^2)\sin\left(\frac{1}{2}\Lambda\cdot TE\right)\sin\left(\frac{1}{2}\Lambda\cdot(t_1-t_2)\right)\right]$
$(2A_yB_z - 2A_zB_y)/2$	$\cos(\pi J\cdot TE)\cdot\left[(2\pi J\delta/\Lambda^2)\sin\left(\frac{1}{2}\Lambda\cdot TE\right)\sin\left(\frac{1}{2}\Lambda\cdot(t_1-t_2)\right)\right]$ $-\sin(\pi J\cdot TE)\cdot\left[(\pi^2J^2\delta/\Lambda^3)\left(2\sin\left(\frac{1}{2}\Lambda\cdot TE\right)\cos\left(\frac{1}{2}\Lambda\cdot(t_1-t_2)\right)-\sin(\Lambda\cdot TE)\right)\right]$

*The symbols are explained in the caption to Table 1.

For citrate at 3 T, $\pi J/\Lambda \cong 0.65$, such that for $n = 3$, Eq. [1] further simplifies to

$$\rho(3\cdot 2\pi/\Lambda) \cong -(A_y + B_y), \qquad [3]$$

This implies that the PRESS spectrum at TE = 242.6 ms will be close to the one sketched in Fig. 1, independently of the particular choice of t_1 and t_2.

Figure 5 shows exemplary in vivo spectra obtained at TE = 100 ms, 110 ms, 120 ms, 130 ms, 140 ms, 250 ms, and 263 ms, with t_1 fixed at 28 ms. They are compared with numerical simulations. The spectra correspond to the points t_2 = 72 ms, 82 ms, 92 ms, 102 ms, 112 ms, 222 ms, and 235 ms in Fig. 2. As expected, at TEs of about $3\cdot 2\pi/\Lambda$, the PRESS sequence produces citrate spectra with strong inner lines whose lineshape is predominantly absorptive.

DISCUSSION

Citrate detection in the prostate is likely to become an important application of in vivo MRS at 3 T (22–26). To make optimal use of the advantages afforded by the higher field, it is necessary to have a thorough understanding of the obtained signal. In the context of in vivo MRS, the full form of the citrate magnetization in response to the PRESS sequence was first discussed by Mulkern and Bowers (5). Wilman and Allen (6) described the signal output of the PRESS sequence (as well as that of the STEAM sequence) in the product operator basis in order to calculate the TE dependence of the total in-phase magnetization along the detection direction $(A_y + B_y)$. While the amplitude of $(A_y + B_y)$ is indeed proportional to the integrated signal, the spectral shape depends on all of the terms. In a different approach, van der Graaf et al. (12,27) calculated the amplitudes and phases of the outer and inner lines indi-

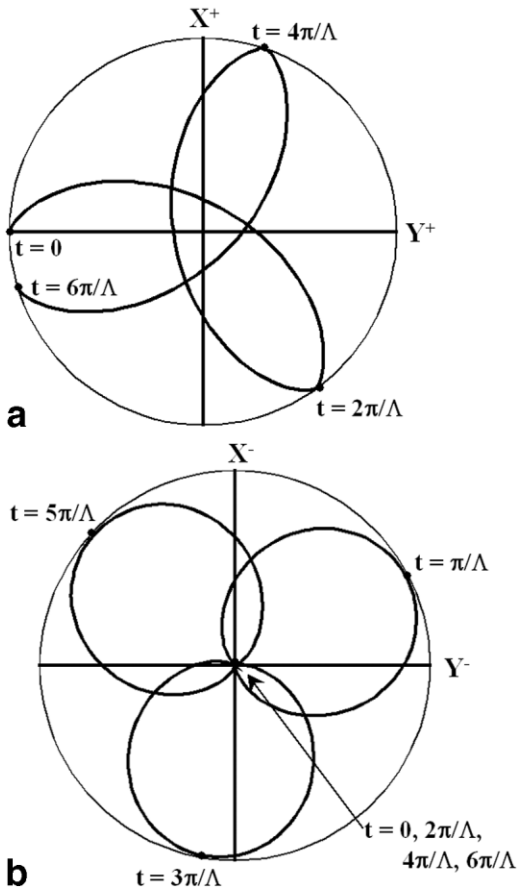

FIG. 4. Parametric plots of the trajectories of the density matrix through the spaces $\{X^+,Y^+\} \equiv \{(A_y + B_y), (2A_xB_z + 2A_zB_x)\}$ (**a**) and $\{X^-,Y^-\} \equiv \{(A_x - B_x), (2A_yB_z - 2A_zB_y)\}$ (**b**). For $0 \le t \le 2\pi/\Lambda$, $t_1 = t$ and $t_2 = 0$; for $2\pi/\Lambda \le t \le 6\pi/\Lambda$, $t_1 = 2\pi/\Lambda$ and $t_2 = t - 2\pi/\Lambda$. Therefore, $t = 6\pi/\Lambda$ corresponds to a PRESS sequence with $t_1 = 2\pi/\Lambda$ = 80.9 ms, and $t_2 = 4\pi/\Lambda$ = 161.8 ms.

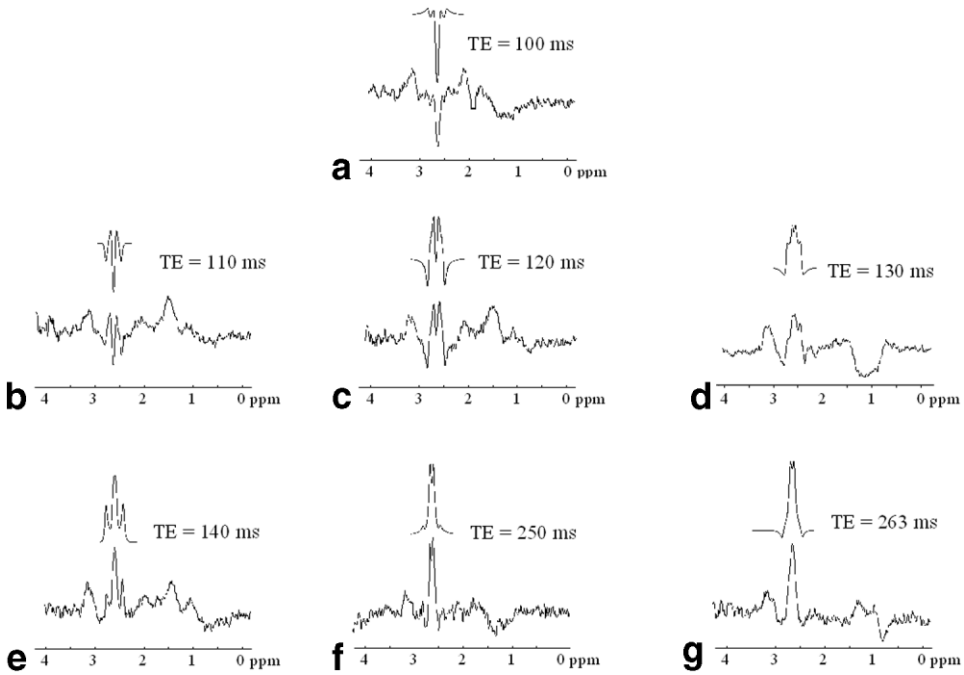

FIG. 5. Real parts of the in vivo spectra acquired with a single-element surface coil (bottom) in comparison with numerical simulations (top). In all experiments t_1 = 28 ms and TR = 1.2 s. The volumes of interest (VOIs) were defined in the central part of the prostate: (**a**) TE = 100 ms (t_2 = 72 ms), VOI: 10.4 ml, 128 averages; (**b**) TE = 110 ms (t_2 = 82 ms), VOI: 12.4 ml, 64 averages; (**c**) TE = 120 ms (t_2 = 92 ms), VOI: 12.4 ml, 80 averages; (**d**) TE = 130 ms (t_2 = 102 ms), VOI: 9.0 ml, 512 averages; (**e**) TE = 140 ms (t_2 = 112 ms), VOI: 12.4 ml, 128 averages; (**f**) TE = 250 ms (t_2 = 222 ms), VOI: 9.0 ml, 512 averages; and (**g**) TE = 263 ms (t_2 = 235 ms), VOI: 9.0 ml, 512 averages.

vidually, with the goal of removing the outer lines of the citrate multiplet (12), which they successfully demonstrated at 1.5 T. Furthermore, they used these results as prior knowledge for fitting algorithms (27).

Here we revisit both approaches and present compact forms of the terms describing the time dependence of all contributions to the total spectrum. These expressions can be easily evaluated on a computer, but also lend themselves to direct "visual" inspection. In the examples given here we focused on concentrating the signal energy in the inner pair of lines, which at most times are stronger than the outer lines. In addition, the outer lines can be obstructed by signals from other metabolites (12). The inner lines' signal preferably should be in-phase (with respect to uncoupled spins) to facilitate quantification and avoid broad dispersion tails interfering with other lines and potentially leading to signal cancellation.

Our analysis revealed that there are indeed TEs providing the desired spectrum. TE = $t_1 + t_2$ = 80.9 ms + 161.7 ms = 242.6 ms was found to yield spectra of favorable appearance. If t_1 is fixed for a given PRESS implementation, TEs somewhat higher than 242.6 ms will produce comparable spectra. In our example the optimum TE was around 250 ms. This value is comparable to the T_2 time of citrate in vivo (25). Therefore, the loss due to transverse relaxation will be substantial. Nevertheless, the spectra shown in Fig. 5f and g demonstrate that even at these long TEs a strong citrate signal can be detected from a 9-ml volume within ~10 min with the use of a single-element surface coil. With the use of coil arrays (22,26), a further reduction in acquisition time can be expected.

On the other hand, long TEs allow one to include selective BASING blocks in the sequence. Furthermore, the accompanying weighting with respect to T_2 yields in general a flatter baseline, and in particular allows for the elimination of signals due to triglyceride from periprostatic fat, which is not affected by the frequency-selective inversion recovery prepulse and may therefore interfere with the citrate signal at 2.6 ppm. This in turn is helpful for signal quantification.

For the sake of completeness, we note that a similar "citrate refocusing" is predicted to occur at 1.5 T for TE = $t_1 + t_2 = 2\pi/\Lambda + 12\pi/\Lambda \cong 107.3$ ms + 643.9 ms = 751.2 ms; at 4 T for TE = $t_1 + t_2 = 2\pi/\Lambda + 2\pi/\Lambda \cong 67.2$ ms + 67.2 ms = 134.4 ms; and at 7 T for TE = $t_1 + t_2 = 2\pi/\Lambda + 4\pi/\Lambda \cong$ 42.9 ms + 85.7 ms = 128.6 ms. The latter two times may be of practical interest. For comparison, an equivalent situation occurs for the signal of the weakly coupled methyl group in lactate at TE = $2/J \cong$ 288.5 ms, independently of field strength. At increasing fields, the optimal value for citrate converges toward TE = $2/J \cong$ 124.2 ms.

As an additional example that is relevant to citrate spectroscopy at 3 T, we briefly mention that for t_1 = 21.0 ms the intensity minima observed for the outer lines go to zero, such that the total signal intensity is focused in the inner pair of lines. At TE = $t_1 + t_2$ = 21 ms + 234 ms = 255 ms, these lines appear to be nearly perfectly in-phase. Furthermore, the analytical results presented here can be helpful in optimizing spectral editing schemes, such as the S-PRESS scheme recently proposed by Gambarota et al. (29). In an elegant fashion, these authors used the fact that the spectral appearance of strongly coupled spin systems can be changed by altering ($t_1 - t_2$) while keeping TE = $t_1 + t_2$ constant.

In the case of "lineshape optimization," the single-transition results (shown in Table 1) provide a direct measure of the spectral appearance of the citrate signal; however, product operators allow for a more comprehensive description of the underlying spin dynamics. For example, we have shown elsewhere (34) that at the "weak points" (TE = $n \cdot 2\pi/\Lambda$) identified here in the dynamics of the AB spin system, it is possible to induce a homonuclear coherence transfer with full efficiency. This allows one, for example, to adapt the "perfect spin echo" (30–33) for strongly coupled spin systems.

For proper sequence optimization, it is crucial to have accurate knowledge of the chemical shift and *J*-coupling values. These values are known to depend on both pH and cation concentrations (3,28). We used the values found by van der Graaf and Heerschap (3) in pH-matched phantom solutions that contained Na^+, K^+, Ca^{2+}, Mg^{2+}, Zn^{2+}, and Cl^- ions in concentrations that reflected the average composition of expressed human prostatic fluid. The satisfactory agreement of the experimental data with the theoretical predictions and numerical simulations in our study even at long TEs indicate the validity of these values at least for healthy tissue. In tumor tissue, potential changes of these values should be kept in mind.

In the present study the PRESS sequence was modeled in a rather crude way. Whereas our model was shown to provide (at least) reliable starting values for optimizing the PRESS experiments, the in vivo spectrum reflects chemical shift evolution during the pulse, varying pulse angles at the edges of the excitation profile, pulse imperfections, off-resonance effects, and potential interference with the BASING elements. In comparison with numerical simulations, the analytical approach pursued here allows for a potentially finer control of the lineshape, particularly when the linewidths become comparable to the spacing between the lines. For example, the spectrum at TE = 100 ms (Fig. 5a) appears at first sight to have the inner lines in phase. However, the results in Fig. 2a indicate that the lines are nearly completely in antiphase. As a consequence, the splitting between the lines is not observed and mutual signal cancellation can lead to decreased peak amplitudes. In situations in which the inner lines are mostly in-phase, the splitting becomes visible (e.g., at TE = 130 ms (Fig. 5d) and TE = 250 ms (Fig. 5f)). In the case of the outer lines, the appearance of which changes quite rapidly with TE (cf., Fig. 2b), the analytical approach avoids the risk of missing interesting features. For example, the spectral appearance of the outer lines changes drastically within 20 ms around t_2 = 100 ms (cf., Fig. 5c–e).

While the output of the PRESS sequence can be readily calculated for weakly coupled spin systems of a basically arbitrary size, the characterization of the signal output for strongly coupled systems is considerably less intuitive, even in the most basic case of a strongly coupled two-spin system. In this work we tried to present and discuss in a comprehensive way all relevant contributions to the PRESS spectrum of citrate at 3 T.

ACKNOWLEDGMENTS

We thank James Murdoch for valuable discussions, and Dr. Malgorzata Marjanska, Prof. Klaas Prüssmann, Rolf Schulte, and Thomas Lange for revising the manuscript.

REFERENCES

1. de Graaf RA. *In vivo* NMR spectroscopy. Principles and techniques. Chichester: John Wiley; 1998.
2. Kurhanewicz J, Swanson MG, Nelson SJ, Vigneron DB. Combined magnetic resonance imaging and spectroscopic imaging approach to molecular imaging of prostate cancer. J Magn Reson Imaging 2002;16:451–463.
3. van der Graaf M, Heerschap A. Effect of cation binding on the proton chemical shifts and the spin-spin coupling constant of citrate. J Magn Reson 1996;B112:58–62.
4. Schick F, Bongers H, Kurz S, Jung WI, Pfeffer M, Lutz O. Localized proton MR spectroscopy of citrate in vitro and of the human prostate in vivo at 1.5-T. Magn Reson Med 1993;29:38–43.
5. Mulkern RV, Bowers JL. Calculating spectral modulations of AB systems during PRESS acquisitions. Magn Reson Med 1993;30:518–519.
6. Wilman AH, Allen PS. The response of the strongly coupled AB system of citrate to typical H-1 MRS localization sequences. J Magn Reson 1995;B107:25–33.
7. Straubinger K, Schick F, Lutz O. Relaxation of AB spin systems in stimulated-echo spectroscopy. J Magn Reson 1995;B109:251–258.
8. Straubinger K, Schick F, Lutz O. Computer-algebra calculations and measurements on AB spin systems for double-spin-echo sequences. Magn Reson Mater Phys Biol Med 1995;3:109–118.
9. Schick F, Straubinger K, Machann J, Nagele T, Bunse M, Klose U, Lutz O. Sequence parameters of double spin-echo sequences affect quantification of citrate. Magn Reson Imaging 1996;14:663–672.
10. Straubinger K, Schick F, Lutz O. Pulse angle dependence of double-spin-echo proton NMR spectra of citrate—theory and experiments. J Magn Reson 1996;B110:188–194.
11. Mulkern RV, Bowers JL, Peled S, Williamson DS. Density-matrix calculations of the 1.5 T citrate signal acquired with volume-localized STEAM sequences. J Magn Reson 1996;B110:255–266.
12. van der Graaf M, Jager GJ, Heerschap A. Removal of the outer lines of the citrate multiplet in proton magnetic resonance spectra of the prostatic gland by accurate timing of a point-resolved spectroscopy pulse sequence. Magn Reson Mater Phys Biol Med 1997;5:65–69.
13. Bottomley PA. Spatial localization in NMR-spectroscopy in vivo. Ann NY Acad Sci 1987;508:333–348.
14. Frahm J, Merboldt KD, Hanicke W. Localized proton spectroscopy using stimulated echoes. J Magn Reson 1987;72:502–508.
15. Schnall M, Lenkinski R, Milestone B, Kressel H. Localized ^{1}H spectroscopy of the human prostate in-vivo. In: Proceedings of the 9th Annual Meeting of SMRM, New York, 1990. p 288.
16. Thomas MA, Narayan P, Kurhanewicz J, Jajodia P, Weiner MW. H-1 MR Spectroscopy of normal and malignant human prostates in vivo. J Magn Reson 1990;87:610–619.
17. Heerschap A, Jager GJ, van der Graaf M, Barentsz JO, Ruijs SHJ. Proton MR spectroscopy of the normal human prostate with an endorectal coil and a double spin-echo pulse sequence. Magn Reson Med 1997;37:204–213.
18. Thompson RB, Allen PS. Sources of variability in the response of coupled spins to the PRESS sequence and their potential impact on metabolite quantification. Magn Reson Med 1999;41:1162–1169.
19. Sørensen OW, Eich GW, Levitt MH, Bodenhausen G, Ernst RR. Product operator-formalism for the description of NMR pulse experiments. Prog Nucl Magn Reson Spectrosc 1983;16:163–192.
20. Kay LE, McClung RED. A product operator description of AB and ABX spin systems. J Magn Reson 1988;77:258–273.
21. Star Lack J, Nelson SJ, Kurhanewicz J, Huang LR, Vigneron DB. Improved water and lipid suppression for 3D PRESS CSI using RF band selective inversion with gradient dephasing (BASING). Magn Reson Med 1997;38:311–321.
22. Kim HW, Buckley DL, Peterson DM, Duensing GR, Caserta J, Fitzsimmons J, Blackband SJ. In vivo prostate magnetic resonance imaging and magnetic resonance spectroscopy at 3 Tesla using a transceive pelvic phased array coil—preliminary results. Invest Radiol 2003;38:443–451.
23. Vigneron DB, Chen A, Cunningham C, Xu D, Hurd R, Sailasuta N, Pauly J, Nelson SJ, Kurhanewicz J. High resolution 3D MR spectroscopic imaging and J-resolved MRS of the prostate at 3 Tesla. In: Proceedings of the 12th Annual Meeting of ISMRM, Kyoto, Japan, 2004. p 386.
24. Cunningham CH, Marjanska M, Chen AP, Xu D, Pauly JM, Sailasuta N, Hurd RE, Kurhanewicz J, Garwood M, Vigneron DB. Sequence design incorporating the LASER technique for prostate MRSI at high field. In: Proceedings of the 12th Annual Meeting of ISMRM, Kyoto, Japan, 2004. p 682.
25. Scheenen T, Gambarota G, Weiland E, Klomp D, Fütterer J, Barentsz J, Heerschap A. Optimal timing for in vivo 1H-MR spectroscopic imaging of the human prostate at 3 Tesla. In: Proceedings of the 12th Annual Meeting of ISMRM, Kyoto, Japan, 2004. p 385.
26. Mao H, Hu X, Heberlein K, Smith R, Torres W. Prostate MRI and MRS at 3 Tesla: using phased surface coil array. In: Proceedings of the 12th Annual Meeting of ISMRM, Kyoto, Japan, 2004. p 942.

27. van der Graaf M, van den Boogaart A, Bovée WMMJ, Heerschap A. Fitting of the AB-type multiplet of citrate using prior knowledge of phase and amplitude modulation. In: Proceedings of the 5th Annual Meeting of ISMRM, Vancouver, Canada, 1997. p 1419.
28. Moore GJ, Sillerud LO. The pH dependence of chemical-shift and spin-spin coupling for citrate. J Magn Reson 1994;B103:87–88.
29. Gambarota G, van der Graaf M, Klomp D, van Asten J, Heerschap A. S-PRESS: a novel approach to difference spectroscopy editing. In: Proceedings of the 12th Annual Meeting of ISMRM, Kyoto, Japan, 2004. p 307.
30. Takegoshi K, Ogura K, Hikichi K. A perfect spin-echo in a weakly homonuclear J-coupled 2 spin-1/2 system. J Magn Reson 1989;84:611–615.
31. van Zijl PCM, Moonen CTW, von Kienlin M. Homonuclear-J refocusing in echo spectroscopy. J Magn Reson 1990;89:28–40.
32. Mulkern RV, Bowers JL, Peled S, Kraft RA, Williamson DS. Citrate signal enhancement with a homonuclear J-refocusing modification to double-echo PRESS sequences. Magn Reson Med 1996;36:775–780.
33. Mulkern RV, Bowers JL, Peled S, Kraft RA, Williamson DS. Citrate signal enhancement with a homonuclear J-refocusing modification to double-echo PRESS sequences (correction). Magn Reson Med 1997;37:477–477.
34. Trabesinger AH, Meier D, Dydak U, Lamerichs R, Boesiger P. Optimizing citrate detection at 3 Tesla. In: Proceedings of the 11th Annual Meeting of ISMRM, Toronto, Canada, 2003. p 760.